Vitrification and levitation of a liquid droplet on liquid nitrogen

Young S. Song[a], Douglas Adler[a], Feng Xu[a], Emre Kayaalp[b,2], Aida Nureddin[c], Raymond M. Anchan[c], Richard L. Maas[d], and Utkan Demirci[a,e,1]

[a]Bio-Acoustic-Microelectromechanical Systems in Medicine Laboratory, Center for Bioengineering, Department of Medicine, Brigham and Women's Hospital, Harvard Medical School, Boston, MA 02115; [b]Faculty of Medicine, Yeditepe University, Istanbul, Turkey 34755; [c]Center for Infertility and Reproductive Surgery, Obstetrics Gynecology and Reproductive Biology, and [d]Division of Genetics, Department of Medicine, Brigham and Women's Hospital, Harvard Medical School, Boston, MA 02115; and [e]Harvard-Massachusetts Institute of Technology Health Sciences and Technology, Cambridge, MA 02139

Edited by Daniel D. Joseph, University of Minnesota, Minneapolis, MN, and approved January 13, 2010 (received for review December 4, 2009)

The vitrification of a liquid occurs when ice crystal formation is prevented in the cryogenic environment through ultrarapid cooling. In general, vitrification entails a large temperature difference between the liquid and its surrounding medium. In our droplet vitrification experiments, we observed that such vitrification events are accompanied by a Leidenfrost phenomenon, which impedes the heat transfer to cool the liquid, when the liquid droplet comes into direct contact with liquid nitrogen. This is distinct from the more generally observed Leidenfrost phenomenon that occurs when a liquid droplet is self-vaporized on a hot plate. In the case of rapid cooling, the phase transition from liquid to vitrified solid (i.e., vitrification) and the levitation of droplets on liquid nitrogen (i.e., Leidenfrost phenomenon) take place simultaneously. Here, we investigate these two simultaneous physical events by using a theoretical model containing three dimensionless parameters (i.e., Stefan, Biot, and Fourier numbers). We explain theoretically and observe experimentally a threshold droplet radius during the vitrification of a cryoprotectant droplet in the presence of the Leidenfrost effect.

cryopreservation | leidenfrost | film boiling | phase change | crystallization

Film boiling is a phenomenon of great interest that has applications in a variety of fields such as aerospace, cryogenics, and electronics. In addition, a similar phenomenon can be easily observed in daily life, e.g., the "dancing droplets" on a frying pan when the droplets come into contact with the pan that is much hotter than the boiling temperature of the droplets (1, 2). The droplets are heated and evaporate on the pan. As a result, they are provided with a levitation force by the generated vapor layer. This solid–liquid film boiling (or liquid–liquid film boiling) is usually caused by a huge temperature distinction between adjacent substances (3–7). Film boiling, also referred to as the Leidenfrost effect, generally impedes the heat transfer between neighboring materials due to the big thermal resistance induced by evaporated vapor layer (8, 9). A great amount of effort has been spent to understand the film boiling behavior of plates or spheres occurring at extremely high temperatures with strong evaporation of a liquid (10–12). On the other hand, when a liquid droplet falls into an extremely cold medium such as a cryogenic fluid (e.g., liquid nitrogen), the relatively hot droplet boils the surrounding medium. Unlike a droplet on the pan, the vapor from the medium, not from the droplet itself, levitates the droplet. Furthermore, abrupt phase change from liquid to solid occurs along with film boiling during cooling down of the droplets.

Here, we investigate the vitrification of a droplet via rapid freezing and its levitation by the Leidenfrost effect. In principle, vitrification implies the phase transition of a liquid to a glass (amorphous ice) with a very low degree of crystallization. To the best of our knowledge, there have been no prior attempts to examine the vitrification behavior of droplets that are ejected directly into liquid nitrogen and the accompanying Leidenfrost phenomenon on the surface of liquid nitrogen. In the current study, we investigate the heat transfer and simultaneous phase change of a nanoliter volume droplet levitating on liquid nitrogen. Understanding the vitrification and film boiling phenomena is also of great importance to other broad applications, such as metallurgy, nuclear reactors, turbine machineries, and biopreservation (13–16). In particular, vitrification is regarded as the only feasible way to successfully cryopreserve human cells and tissues such as oocytes and brain tissue (17, 18).

Upon ejecting a droplet into liquid nitrogen, as demonstrated in Fig. 1*A*, the liquid nitrogen surrounding the droplet absorbs the heat from the liquid of relatively higher temperature and evaporates (14, 15, 19, 20). As soon as droplets are immersed in liquid nitrogen, the evaporated nitrogen results in a buoyant force and a pressure differential pushing droplets to the liquid nitrogen surface (i.e., levitation phenomenon; Fig. S1 and Video S1). This levitation continues until the droplet temperature reaches the Leidenfrost temperature (Fig. 1*D*; Video S1). Assuming that the static feature of the droplet primarily governs the entire system [as first reported by Frederking and Clark (21)], the flow behavior of nitrogen gas environing a droplet and following pressure development can be analytically modeled as an incompressible flow in cavities, Fig. 1*B* and *C* (also see *SI Text*). The vapor blanket acts as a heat-insulating layer, thereby hindering heat transfer for cooling.

Results and Discussion

Once the temperature of a liquid approaches its freezing point, solidification of the liquid (crystallization or vitrification) starts depending on cooling conditions such as cooling rate, nucleation sites, and pressure (22–24). To describe such a solidification process, two models, i.e., the Stefan and zone models, have been employed (25). Unlike the Stefan model, where the entire domain is sharply divided into solid and liquid subdomains by a moving phase interface, the zone model benefits from more efficiency in characterizing the crystallization process using a propagating zone. In the current study, the zone model is adopted by using the following nonisothermal kinetic equation proposed by Boutron and Mehl (13):

$$\frac{d\chi}{dt} = k_a \chi^{\frac{2}{3}}(1-\chi)(T_f - T)e^{-Q/RT} \qquad [1]$$

Author contributions: U.D. designed research; Y.S.S. and D.A. performed research; F.X., E.K., A.N., R.M.A., R.L.M., and U.D. analyzed data; and Y.S.S., F.X., and U.D. wrote the paper.

The authors declare no conflict of interest.

This article is a PNAS Direct Submission.

Freely available online through the PNAS open access option.

[1]To whom correspondence should be addressed. E-mail: udemirci@rics.bwh.harvard.edu.

[2]Present address: Jamaica Hospital Medical Center, 8900 Van Wyck Expressway, Jamaica, NY 11418.

This article contains supporting information online at www.pnas.org/cgi/content/full/0914059107/DCSupplemental.

where χ is the degree of ice crystallization ($0 < \chi < 1$), t (s) is time, Q (J/mol) is the activation energy, T_f (K) is the final temperature of the freezing process, R (J/mol K) is the gas constant, and k_a is a characteristic constant. In the case of a spherical-shaped droplet, $k_a = \frac{L}{\pi\delta^2\nu T_f r_f}$, where L (J/kg) is the latent heat, δ (m) is the thickness of the transition layer between liquid phase and solid phase, r_f (m) is the radius of ice region, and ν (m^2/s) is the kinematic viscosity. This zone model is based on the hypothesis that the sum of specific and latent heats can be given by an enthalpy function (13, 23).

The primary mode of heat transfer in the droplet at cryogenic temperatures is heat conduction rather than heat convection, as the Peclet number with physical meaning of the ratio of convection to conduction in the convecting region, $Pe = DV_{\text{in}}/\alpha \ll 1$ [D is characteristic length, i.e., the diameter for spherical droplets, V_{in} is the internal flow velocity of liquid within droplets, $\alpha = \frac{\lambda}{\rho c_p}$ is the thermal diffusivity with unit of m^2/s, ρ (kg/m^3) is density, c (J/kg K) is specific heat, and λ (W/m K) is thermal conductivity]. Dimensional analysis is carried out using corresponding characteristic quantities as explained below: characteristic time (heat diffusion time) $t_c = R^2/\alpha$ with unit of second, dimensionless radius $r^* = r/R$, where R is the radius of the droplet and r is the coordinate in the radius direction, dimensionless time (Fourier number) $t^* = t/t_c (= Fo)$ indicating the ratio of the heat conduction rate to the rate of thermal energy storage, and dimensionless temperature $T^* = \frac{T-T_\infty}{T_i-T_\infty}$, in which T_i (K) is the initial temperature of droplets, and T_∞ (K) is the temperature of liquid nitrogen. The resulting heat transfer equation is expressed as

$$\frac{\partial T^*}{\partial t^*} = \nabla^2 T^* + St\frac{\partial \chi}{\partial t^*} \quad [2]$$

in which ∇ is a differential vector operator and St denotes the Stefan number $St = \frac{L}{c_p(T_i-T_\infty)}$ [L (kJ/kg) is the heat of fusion] indicating the ratio of sensible heat to latent heat. The imposed boundary conditions are as follows: $\frac{\partial T^*}{\partial r^*} = 0$, at $r^* = 0$ (at the center of droplets) and $\frac{\partial T^*}{\partial r^*} = -BiT^*$ at $r^* = 1$ (at the surface of droplets). Here $Bi = \frac{hR}{\lambda}$, where h denotes the convective heat transfer coefficient ($W/m^2 K$) indicating the ratio of the heat transfer resistances inside and at the surface of a body. The initial condition of $T = T_i$ at $t = 0$ is applied. The distinguishing characteristic of a

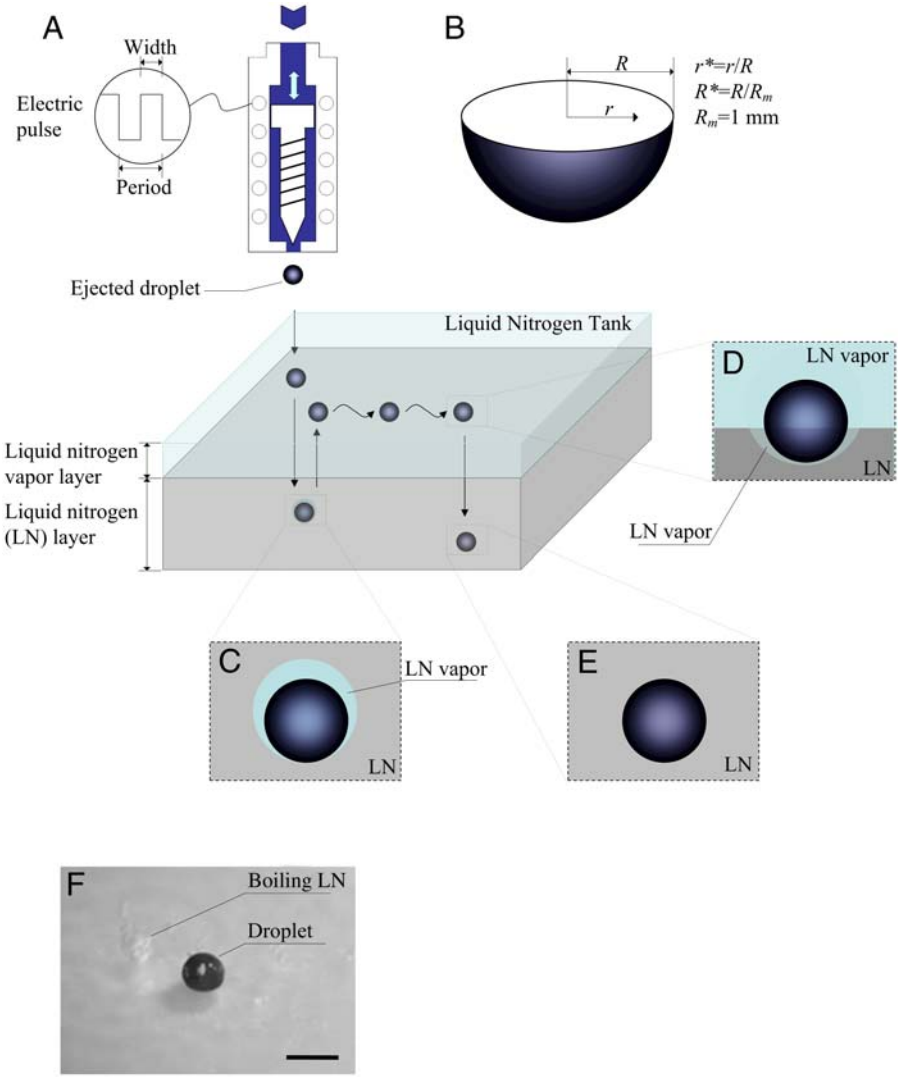

Fig. 1. Generation and levitation of droplets on top of liquid nitrogen. (*A*) A schematic description of the experimental setup and of the behavior of droplets over time. It is a cross-sectional image of the ejector that is driven by an electric pulse. (*B*) Schematic demonstration of a droplet in the liquid nitrogen. The droplet in dark blue color is surrounded by the liquid nitrogen vapor as shown in the schematic drawing. (*C*) Schematic illustration of a droplet floating around on top of liquid nitrogen. (*D*) Photograph of a droplet levitating on liquid nitrogen. The droplet stained with a color dye is partially submerged in the liquid nitrogen as illustrated in *C*. (Scale bar, 1 mm.)

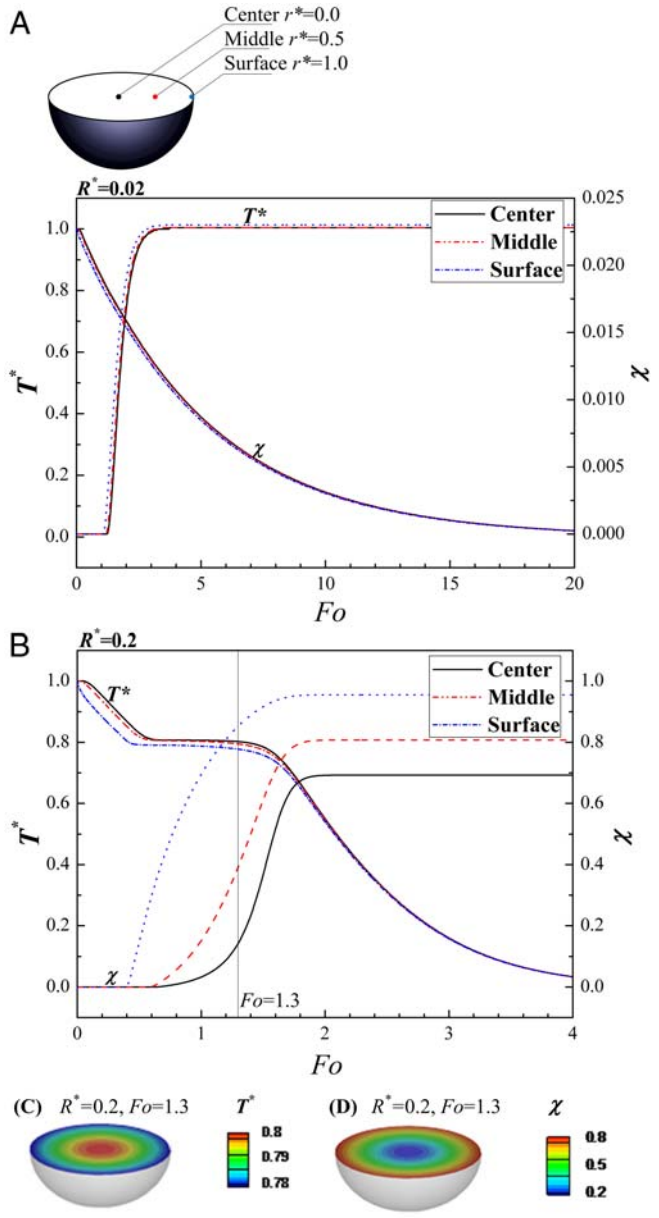

Fig. 2. Change in temperature and degree of crystallization as a function of time. (*A*) Plot of the dimensionless temperature and crystallinity for a droplet with a dimensionless radius of 0.02. The left-hand and right-hand axes of the graph denote the dimensionless temperature and degree of crystallinity, respectively. (*B*) Change in the dimensionless temperature and degree of crystallization for a droplet with a dimensionless radius of 0.2 with respect to the dimensionless time, *Fo*. (*C*) Profile of the dimensionless temperature at $Fo = 1.3$. (*D*) Contour of the degree of crystallization at $Fo = 1.3$.

phase transition is an abrupt change in thermophysical properties, in particular the thermal conductivity (k), heat capacity (c_p), and density (ρ), with respect to a thermodynamic variable such as temperature. In our calculations, these temperature-dependent properties are considered (13, 26).

The predicted temperature variations and degree of crystallization are demonstrated at three locations inside the droplet (center, middle, and surface) as shown in Fig. 2*A* and *B*. The radius of droplets is normalized as $R^* = R/R_m$, where R_m is the maximum radius (1×10^{-3} m) considered in this study. A small droplet with a dimensionless radius $R^* = 0.02$ ($R = 20$ μm) cools down quickly due to its low heat capacity (Fig. 2*A*). As a result, it has a small degree of crystallization ($\chi \approx 0.023$). In contrast, the temperature plot of a droplet with a dimensionless radius $R^* = 0.2$ ($R = 200$ μm) has a plateau regime due to the latent heat caused by crystallization of liquid (Fig. 2*B*). As seen in Fig. 2*A* and *B*, the ice crystal formation in the two droplets stops at a dimensionless temperature of approximately $T^* = 0.56$ (i.e., $T \approx 200$ K) during cooling. It is known that the total degree of crystallization depends on how quickly the droplets pass the dangerous temperature region (DTR) (13). Therefore, shortening the time duration passing through the DTR is critical to minimize ice crystal formation and improve vitrification during rapid cooling. Because the surface of a droplet comes in contact with liquid nitrogen first, it cools down more quickly than the inner regions (Fig. 2*A* and especially Fig. 2*B*). However, the surface (or outer region) takes more time to pass through the DTR than the inner regions due to the latent heat flowing radially outward from the inner region to the outer region of the droplet, thereby generating more ice crystals in the outer region (Fig. 2*B*) (27). Fig. 2*C* and *D* present the profiles of temperature and crystallinity across the 200 μm droplet at *Fo* of 1.3, which was chosen to clearly see the difference of the crystallinity arbitrarily. Because the internal thermal resistance of the droplet is smaller than the external thermal resistance between droplet surface and liquid

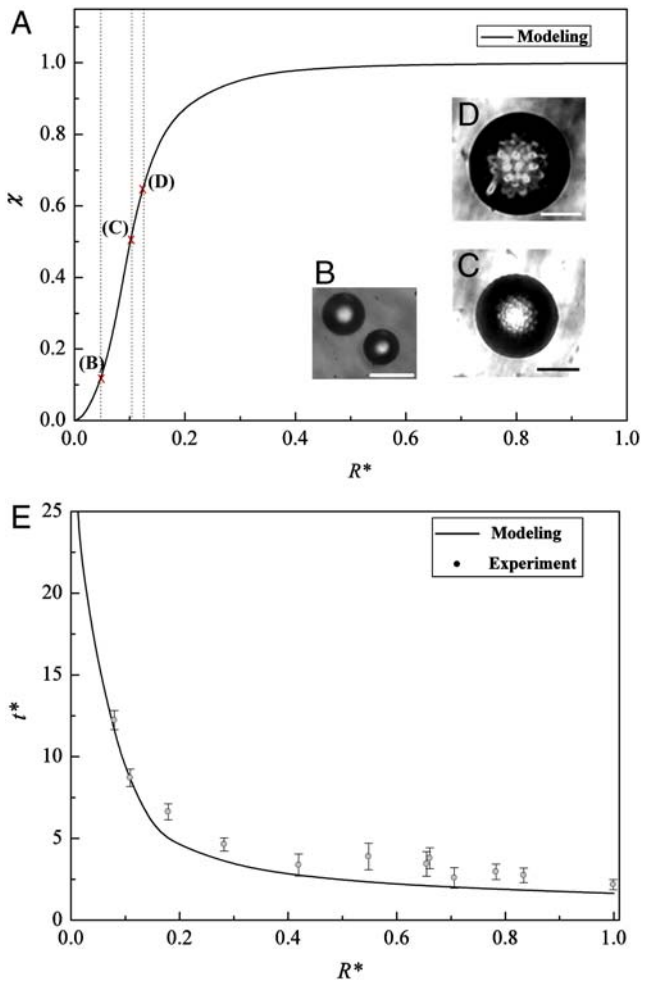

Fig. 3. Variation in the degree of crystallization and dimensionless Leidenfrost time as a function of the radius. (*A*) Plot of the crystallinity vs. the dimensionless radius. (*B–D*) Images of droplets in liquid nitrogen. (Scale bar, 100 μm.) (*E*) Graph of the dimensionless Leidenfrost time vs. the dimensionless radius. The dimensionless Leidenfrost time is defined as t_{LF}/t_c, in which t_{LF} is the Leidenfrost time.

nitrogen ($Bi < 1$, i.e., heat transfer occurs faster inside the droplet), the range of the temperature variation across the droplet is narrow (Fig. 2*C*).

After calculating the final degree of crystallization of a droplet, we averaged the value using the relevant volume. The calculated degree of crystallization of droplets is found to be a strong function of the droplet size (Fig. 3*A*). As the droplet radius increases, the degree of crystallization also increases, especially between 0 and 0.2 dimensionless radii. The droplets with a low degree of crystallization after cooling can be regarded as vitrified droplets. During cooling, homogeneous ice nucleation first happens between homogeneous nucleation temperature T_h and the melting temperature T_m (e.g., $-42 \sim 0\,^{\circ}\mathrm{C}$ for water), followed by heterogeneous ice nucleation in the range of the glass transition temperature (T_g) to T_h (28). In the nucleation regimes, including the DTR as shown in Fig. 2*A* and *B*, the probability for a volume of ice crystal (V) can be given by $J(T,P) \times V \times \Delta t$, where $J(T,P)$ is the nucleation rate as a function of temperature T and pressure P (29). Rapid cooling can shorten the time duration in the nucleation regime (Δt), thus decrease the probability of ice crystal nucleation. For instance, a cooling rate of $\sim 10^8\,^{\circ}\mathrm{C}/\mathrm{min}$ allows the vitrification of pure water (30). It is noted that there exists a critical droplet size beyond which incipient nuclei grow leading to the formation of ice crystals. Otherwise, incipient nuclei collapse and an ice crystal is not created. The thermodynamic characteristic temperatures (T_g, T_h, and T_m) change along with the composition and concentration of solutes. In the current study, we took into account of cryoprotective agents (CPAs), which are chemicals used to minimize damage of cells or tissues during freezing. T_h and T_m decrease, while T_g increases, with increasing CPA concentration. By increasing CPA concentration, T_g and T_m become closer and eventually meet. As a result, a vitrified solid can be generated even at a slow cooling rate in the case of ~60% wt/wt of CPAs (31). Fig. 3*B–D* shows the frozen droplets in the liquid nitrogen. As the droplet size increases, morphological changes are observed: Vitrified droplets are translucent with bright cores (Fig. 3*B*), but crystallized droplets contain granular particles inside (ice crystals) (Fig. 3*C* and *D*). In addition, it is shown that the large droplets have grain-like crystal particles due to the longer cooling time. The experimental results shown in Fig. 3*B–D* are found to be consistent with the numerical findings.

Fig. 3*E* demonstrates the hovering time of droplets on liquid nitrogen. When droplets plummet into liquid nitrogen, three regimes are defined: a film boiling regime, a transition boiling regime, and a nucleate boiling regime. The evaporation rate of film boiling is known to be lower than that of peak nucleate boiling by more than one order of magnitude (14). During the transition from film boiling to nucleate boiling, the vapor blanket surrounding the droplet disappears. Subsequently, the droplet sinks beneath the liquid nitrogen. The temperature at the moment that film boiling changes into nucleate boiling corresponds to the Leidenfrost temperature. The hovering time is the elapsed time when the calculated temperature of droplets reaches the Leidenfrost temperature. The Leidenfrost time normalized by the diffusive characteristic time (t_c) declines dramatically and approaches an asymptotic value (~1.5). As the size of the droplet increases, the influence of heat diffusion in the droplet strengthens. It is interpreted that the smaller droplets are more easily affected by external heat transfer than by internal heat diffusion because the Biot number (Bi) gets smaller ($\ll 1$). Similar to the change in crystallinity (Fig. 3*A*), the dimensionless Leidenfrost time drastically alters between 0 and ~0.2 (Fig. 3*E*). Please note that thermodynamics and heat transfer between the droplet and liquid nitrogen modeled in this study play a more important role in determining the vitrification behavior and hovering time of the droplet than relevant hydrodynamics. The hydrodynamics of the convection film boiling is explained in *SI Text*. In addition, the experimental and numerical results show the same trends (Fig. 3*E*).

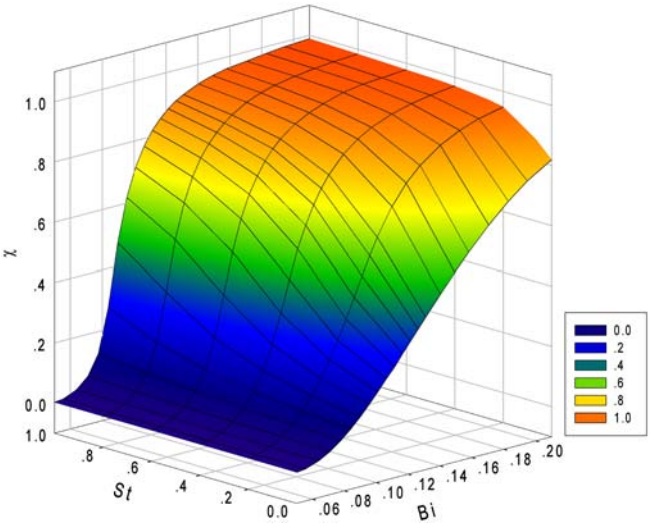

Fig. 4. Plot of the degree of crystallization in the domain of the *St* and *Bi* numbers. The degree of crystallization increases with an increase in the *St* and *Bi* numbers. In particular, the degree of crystallization drastically rises with respect to the *Bi* number.

By using two governing dimensionless parameters (i.e., *Bi* and *St*) in our system, we analyzed the characteristics of crystallization of droplets (i.e., χ). That is, the degree of crystallization increases with an increase in either *St* or *Bi* (Fig. 4). In particular, we find that the crystallinity is a stronger function of *Bi* than *St*. This is attributed to the fact that the heat transfer at the interface between the droplets and the liquid nitrogen is more critical in determining the crystallization of droplets than the internal heat capacity of the droplets. Here, it is noted that, in the case of $St = 0$, it is identical to the uncoupled approach, where the energy equation [**2**] is decoupled from the kinetics of ice crystal formation (Eq. **1**) (27).

In summary, we have theoretically analyzed the vitrification and Leidenfrost phenomena of droplets in liquid nitrogen using dimensionless physical parameters and compared the theoretical results with experimental data. This dimensionless analysis explains the simultaneous levitation and phase change of droplets.

Methods

Experimental Methods. A valve-based droplet ejector with nozzle diameter 150 μm (SMLD-5b, TechElan) was connected to a syringe through a needle and tubing, and the liquid was then loaded into the syringe. The air line was connected to the syringe to provide a pressure of 34 kPa to overcome the surface tension of a droplet at the orifice of the ejector (Fig. 1*A*). The ejector was controlled by a pulse generator (8112A 50 MHz, Hewlett-Packard). Droplets are generated to implement rapid cooling by using an air-pressure, pulse-controlled solenoid valve. Larger droplets were generated using a micropipette. Cryoprotectant, 3 M 1,2-propanediol (PrOH, EMD Chemicals), was employed to vitrify droplets. Blue food dye was used to stain the droplets. The generated droplets were plunged into a liquid nitrogen bath (glass Petri dishes, Pyrex). The liquid nitrogen container was covered with aluminum foil in a bid to prevent possible electrostatic interactions between the container and droplets. Right after the immersion of droplets, the levitation time of the droplets was measured until they sank into the liquid nitrogen bath. The frozen droplets were taken for imaging (Spot Advanced, Diagnostic Instruments, Inc.) under a microscope (Eclipse Ti-S, Nikon) using a polarized filter. Droplet sizes were measured based on recorded images.

Numerical Simulations. Finite element simulation was carried out to model the heat transfer, phase change, and Leidenfrost phenomena of droplets. To predict the temperature and degree of crystallization of droplets during cooling, we simultaneously calculated Eqs. **1** and **2** because they are coupled to each other. For the calculation, we assumed a spherical symmetry based on

the analytical solutions of fluid dynamics of the nitrogen vapor (*SI Text*). The fourth-order Runge–Kutta algorithm and the backward Euler method, which is an implicit method solving an equation set to move forward to a next time step during calculation, were employed for the numerical simulations.

ACKNOWLEDGMENTS. We would like to thank Dr. Can Erdonmez, Dr. Edward Haeggstrom, Dr. Sangjun Moon, Naside Gozde Durmus, Onur Hasan Keles, and Dr. Ragip Akbas for feedback and discussions. This work was supported by National Institutes of Health Grant R21 EB007707. U.D. was partially supported by R01-AI081534. R.L.M. and R.M.A. were supported by 1RL1 DE019021. This work was performed at the Bio-Acoustic Microelectromechanical Systems in Medicine Laboratories, Center for Bioengineering, Brigham and Women's Hospital, Harvard Medical School and Harvard-Massachusetts Institute of Technology Health Sciences and Technology.

1. Quere D, Ajdari A (2006) Liquid drops surfing the hot spot. *Nat Mater* 5:429–430.
2. Linke H, et al. (2006) Self-propelled Leidenfrost droplets. *Phys Rev Lett* 96 (15):1545021–1545024.
3. Biance AL, Clanet C, Quere D (2003) Leidenfrost drops. *Phys Fluids* 15(6):1632–1637.
4. Bhat SN, Sharma A, Bhat SV (2005) Vitrification and glass transition of water: Insights from spin probe ESR. *Phys Rev Lett* 95(23):2357021–2357024.
5. Tso CP, Low HG, Ng SM (1990) Pool film boiling from spheres to saturated and subcooled liquids of Freon-12 and Freon-22. *Int J Heat Mass Tran* 11:154–159.
6. Honda H, Makishi O, Yamashiro H (2007) Generalized stability theory of vapor film in subcooled film boiling on a sphere. *Int J Heat Mass Tran* 50:3390–3400.
7. Dhir VK, Purohit GP (1978) Subcooled film-boiling heat transfer from spheres. *Nucl Eng Des* 47:49–66.
8. Gottfried BS, Lee CJ, Bell KJ (1966) The Leidenfrost phenomenon: Film boiling of liquid droplets on a flat plate. *Int J Heat Mass Tran* 9:1167–1187.
9. Son G, Dhir VK (2008) Three-dimensional simulation of saturated film boiling on a horizontal cylinder. *Int J Heat Mass Tran* 51:1156–1167.
10. Yuan MH, Yang YH, Li TS, Hu ZH (2008) Numerical simulation of film boiling on a sphere with a volume of fluid interface tracking method. *Int J Heat Mass Tran* 51:1646–1657.
11. Kolev NI (1998) Film boiling on vertical plates and spheres. *Exp Therm Fluid Sci* 18:97–115.
12. Tso CP, Leong KC, Tan HS (1995) An analysis of natural convection film boiling from spheres using the spherical coordinate system. *Int Comm Heat Mass* 22:803–813.
13. Boutron P, Mehl P (1990) Theoretical prediction of devitrification tendency: Determination of critical warming rates without using finite expansions. *Cryobiology* 27 (4):359–377.
14. Bernardin JD, Mudawar I (2004) A Leidenfrost point model for impinging droplets and sprays. *J Heat Transf* 126(2):272–278.
15. Prusa J, Yao LS (1985) Effects of density change and subcooling on the melting of a solid around a horizontal heated cylinder. *J Fluid Mech* 155:193–212.
16. Xie H, Zhou Z (2007) A model for droplet evaporation near Leidenfrost point. *Int J Heat Mass Tran* 50:5328–5333.
17. Fahy GM (1986) *Vitrification: A New Approach to Organ Cryopreservation* (Alan R. Liss, New York).
18. Fahy GM, Levy DI, Ali SE (1987) Some emerging principles underlying the physical properties, biological actions, and utility of vitrification solutions. *Cryobiology* 24:196–213.
19. Hsiao KH, Witte LC, Cox JE (1975) Transient film boiling from a moving sphere. *Int J Heat Mass Tran* 18:1343–1350.
20. Demirci U, Montesano G (2007) Cell encapsulating droplet vitrification. *Lab Chip* 7(11):1428–1433.
21. Frederking THK, Clark JA (1963) Natural convection film boiling on a sphere. *Adv Cryog Eng* 8:501–506.
22. Ren HS, Wei Y, Hua TC, Zhang J (1994) Theoretical prediction of vitrification and devitrification tendencies for cryoprotective solution. *Cryobiology* 31:47–56.
23. Benard A, Advani SG (1995) Energy equation and the crystallization kinetics of semi-crystalline polymers: regimes of coupling. *Int J Heat Mass Tran* 38:819–832.
24. Le Bot C, Delaunay D (2008) Rapid solidification of indium: modeling subcooling. *Mater Charact* 59:519–527.
25. Astarita G, Kenny JM (1987) The Stefan and Deborah numbers in polymer crystallization. *Chem Eng Commun* 53:69–84.
26. Cui ZF, Dykhuizen RC, Nerem RM, Sembanis A (2002) Modeling of cryopreservation of engineered tissues with one-dimensional geometry. *Biotechnol Prog* 18:354–361.
27. Jiao A, Han X, Critser JK, Ma H (2006) Numerical investigation of transient heat transfer characteristics and vitrification tendencies in ultra-fast cell cooling process. *Cryobiology* 52:386–392.
28. Debenedetti PG, Stanley HE (2003) Supercooled and glassy water. *Phys Today* 56:40–46.
29. Lee RE, Jr, Warren GJ, Gusta LV (1995) *Biological Ice Nucleation and its Applications* (APS Press, St. Paul, MN).
30. Johair GP, Hallbrucker A, Mayer E (1987) The glass-liquid transition of hyperquenched water. *Nature* 330:552–553.
31. Arav A, et al. (2002) New trends in gamete's cryopreservation. *Mol Cell Endocrinol* 187:77–81.